Molecular Pharmacology Fast Forward. Published on October 19, 2015 as DOI: 10.1124/mol.115.098228
This article has not been copyedited and formatted. The final version may differ from this version.

Title Page

Reduced myelination and increased glia reactivity resulting from severe neonatal hyperbilirubinemia.

Andreia Barateiro, Shujuan Chen, Mei-Fei Yueh Adelaide Fernandes, Helena Sofia Domingues, João Relvas, Olivier Barbier, Nghia Nguyen, Robert H. Tukey, and Dora Brites.

Research Institute for Medicines (iMed.UL), Faculdade de Farmácia, Universidade de Lisboa, Av. Professor Gama Pinto, 1649-003 Lisbon, Portugal. (AP, AF, DB)

Laboratory of Environmental Toxicology, Department of Pharmacology, and Chemistry & Biochemistry, University of California San Diego, 9500 Gilman Drive, La Jolla, CA 92093-0722, USA. (SC, MFY, NN, RHT)

*Department of Biochemistry and Human Biology, Faculty of Pharmacy, University of Lisbon, Av. Professor Gama Pinto, 1649-003 Lisbon, Portuga*l. (AF, DB)

Departamento de Biologia Experimental, Faculty of Medicine, University of Porto, Av. Prof. Hernâni Monteiro, 4200-319 Porto, Portugal. (SD, JR)

Instituto de Biologia Molecular e Celular, University of Porto, Rua do Campo Alegre 823, 4150-180 Porto, Portugal. (JR)

Laboratory of Molecular Pharmacology, Centre hospitalier universitaire de Quebec Reserach Center and the Faculty of Pharmacy, Laval University, Quebec, QC, Canada G1V 4G2. (OB)

Molecular Pharmacology Fast Forward. Published on October 19, 2015 as DOI: 10.1124/mol.115.098228
This article has not been copyedited and formatted. The final version may differ from this version.

Running Title Page: "Kernicterus results in myelination defects"

***Corresponding authors:**

Dora Brites, Ph.D.

Research Institute for Medicines, Faculdade de Farmácia, Universidade de Lisboa, Av. Professor Gama Pinto, 1649-003 Lisbon, Portugal, Email: dbrites@ff.ulisboa.pt

Robert H. Tukey, Ph.D.

UC San Diego, Leichtag Biomedical Research Building, 9500 Gilman Drive, La Jolla, California, USA. 92093-0722. E-mail address: rtukey@ucsd.edu

Number of text pages:33

Number of Tables: 0

Number of Figures: 7

Number of References: 37

Number of words in Abstract: 241

Number of words in the Introduction: 618

Number of words in the Discussion: 1,460

Molecular Pharmacology Fast Forward. Published on October 19, 2015 as DOI: 10.1124/mol.115.098228
This article has not been copyedited and formatted. The final version may differ from this version.

Abbreviations: BIND, bilirubin-induced neurological dysfunction; BSA, bovine serum albumin; CC-1, Adenomatous Polyposis Coli; ES cells, embryonic stem cells; GFP, glial fibrilar acidic protein; HPLC, high-performance liquid chromatography; Iba, ionized calcium binding adaptor molecule; IL, interleukin; MBP, myelin basic protein; MLM, mouse liver microsomes; MSIM, mouse small intestinal microsomes; PBS, phosphate buffer saline; qRT-PCR, quantitative reverse transcription polymerase chain reaction; RT, room temperature; TLR2, Toll-like receptor 2; TNF, tumor necrosis factor; TSB, total serum bilirubin; *UFP*, mice homozygous for the *Ugt1a1*$^{LoxP[FRTneoFRT]LoxP}$ allele; *UAC*, *UFP/albumin-Cre* mice; UCB, unconjugated bilirubin; UDPGA, UDP-glucuronic acid; UGT, UDP-glucuronosyltransferase.

Molecular Pharmacology Fast Forward. Published on October 19, 2015 as DOI: 10.1124/mol.115.098228
This article has not been copyedited and formatted. The final version may differ from this version.

Abstract

Bilirubin-induced neurologic dysfunction (BIND) and *kernicterus* has been used to describe moderate to severe neurological dysfunction observed in children exposed to excessive levels of total serum bilirubin (TCB) during the neonatal period. Here we use a new mouse model that targets deletion of the *Ugt1* locus and the *Ugt1a1* gene in liver to promote hyperbilirubinemia induced seizures and CNS toxicity. The accumulation of TCB in these mice leads to diffuse yellow coloration of brain tissue and a marked cerebellar hypoplasia that we characterize as kernicterus. Histological studies of brain tissue demonstrate that the onset of severe neonatal hyperbilirubinemia, characterized by seizures, leads to alterations in myelination and glia reactivity. Kernicterus presents axonopathy with myelination deficits at different brain regions including pons, medulla oblongata and cerebellum. The excessive accumulation of TSB in the early neonatal period (5-days after birth) promotes activation of the myelin basic protein (*Mbp*) gene with an accelerated loss of MBP that correlates with a lack of myelin sheath formation. These changes were accompanied by increased astroglial and microglial reactivity, possibly as a response to myelination injury. Interestingly, cerebellum was the most affected area with greater myelination impairment and glia burden, showing a marked loss of Purkinje cells and a reduced arborization of the remaining ones. Thus, kernicterus in this model displays not only axonal damage but also myelination deficits and glial activation in different brain regions that are usually related to the neurological sequelae observed after severe hyperbilirubinemia.

Molecular Pharmacology Fast Forward. Published on October 19, 2015 as DOI: 10.1124/mol.115.098228
This article has not been copyedited and formatted. The final version may differ from this version.

Introduction

Hyperbilirubinemia is a common clinical condition occurring in the neonatal period. Over 60% of term and virtually all premature infants experience temporary, mild to moderate "physiological" jaundice, due to excessive production of unconjugated bilirubin (UCB) and defective bilirubin clearance (Stevenson et al., 2001;Cohen et al., 2010). In the vast majority of cases neonatal jaundice represents a benign condition, but in some newborns the concentration of serum bilirubin may increase with passage of the pigment into brain causing various degrees of acute or chronic bilirubin induced neurological dysfunction (BIND) which can expand to UCB-induced encephalopathy (kernicterus) (Shapiro, 2003;Shapiro, 2005;Shapiro, 2010). In this situation bilirubin leads to cellular neuroinflammation with activation of astrocytes and microglia, as well as gliosis. (Shapiro, 2005;Yueh et al., 2014;Johnson and Bhutani, 2011;Brites, 2012). The bench mark of extreme bilirubin neurotoxicity or kernicterus is an irreversible posticteric sequelae, presented as icteric or yellow staining of brain tissue resulting from the accumulation of UCB in selective regions of the brain (Johnson and Bhutani, 2011). Hence, it is important to understand the molecular mechanisms by which bilirubin exerts such neurodevelopmental abnormalities.

Humanized *UGT1* (*hUGT1*) mice express the human *UGT1* locus in a *Ugt1*-null background (Fujiwara et al., 2010). Mutation of the *Ugt1* locus by interruption of exon 4 in the common region of the *Ugt1a1* gene leads to inactivation of the UGT1A proteins, including UGT1A1 (Nguyen et al., 2008). Since UGT1A1 is the only glucuronosyltransferase responsible for the glucuronidation of bilirubin (Bosma et al., 1994), *Ugt1*$^{-/-}$ mice accumulate high levels of UCB, resulting in neonatal lethality approximately one week after birth. Incorporating the human *UGT1* locus through transgenic technology into the *Ugt1*-null background leads to recovery of neonatal

Molecular Pharmacology Fast Forward. Published on October 19, 2015 as DOI: 10.1124/mol.115.098228
This article has not been copyedited and formatted. The final version may differ from this version.

lethality, although the new born *hUGT1* mice all display severe hyperbilirubinemia (Fujiwara et al., 2010). Approximately 10% of neonatal *hUGT1* mice progress into seizures, succumbing to CNS toxicity as evident by accumulation of bilirubin in brain tissue. The stark accumulation of bilirubin in brain tissue coincides with neuroinflammation and reactive gliosis, a term we have defined as "kernicterus" in these mice, which we have also found linked to Toll-like receptor 2 (TLR2) control of bilirubin induced signaling (Yueh et al., 2014). TRL2 mediated gliosis correlated with the development of a bilirubin induced pro-inflammatory environment with upregulation of inflammatory markers such as TNFα, IL-1β and IL-6 in the CNS. Expression of TRL2 is a key intermediate in regulating the onset of BIND, since deleting the *Tlr2* gene in *hUGT1* mice leads to a dramatic increase in the neonatal death rate in *hUGT1/Trl2*$^{-/-}$ mice. These findings represent the first mechanistic link between hyperbilirubinemia and the CNS toxicity, demonstrating that TLR2 signaling and microglia-associated neuroinflammation are linked to a repair and protection mode against BIND.

The early onset of hyperbilirubinemia during the neonatal period in *hUGT1* mice is identified by severely elevated levels of total serum bilirubin (TSB) that coinside with the onset of seizures. While approximately 1 in 10 *hUGT1* mice develop these symptoms (Fujiwara et al., 2010), we sought to develop a more consistent mouse model to examine the impact of hyperbilirubinemia on gliosis and CNS damage. This was accomplished by using the *Cre/loxP* system (Lewandoski, 2001) to target the deletion of the *Ugt1a1* gene in liver tissue. All of these mice develop elevated TSB levels that occur during neonatal development. This condition results in the development of kernicterus with a visible reduction in cerebellum volume. Microscopically, kernicterus formation presents a reduced number of axons and reduced myelination in different

Molecular Pharmacology Fast Forward. Published on October 19, 2015 as DOI: 10.1124/mol.115.098228
This article has not been copyedited and formatted. The final version may differ from this version.

brain regions. In parallel, myelination impairment was associated with increased astroglial and microglial reactivity in the same brain regions. The development of kernicterus in these mice provides important new clues toward understanding the early events leading to neonatal toxicity by bilirubin.

MATERIAL AND METHODS

Generation of the kernicterus mouse model. The targeting construct consisted of a phosphoglycerine kinase (PGK)-Neomycin resistance gene cassette (PGK-neo) that was flanked by *Flp/FRT* recombinase sites in the intron region between exons 3 and 4 fo the *Ugt1a1* gene. Positioned in intron 2 and then again outside of the *Flp/FRT* recombinase sites are positioned *Cre/loxP* recombinase sites. This construct was electroporated into ES cells, and neomycin positive clones were injected into C57BL/6 blastocysts. The chimera mice were out-crossed with wild type C57BL/6 mice for five generations, and then in-bred to generate mice homozygous for the $Ugt1^{LoxP[FRTneoFRT]LoxP}$ allele. These mice were identified as *UFP* mice. To delete exons 3 and 4 in liver tissue, *UFP* mice were crossed with mice that express as a transgene a*lbumin-Cre*, generating UFP/*albumin-Cre* mice, and were designated as *UAC* mice. Deletion of the *Ugt1a1* exons 3 and 4 in liver tissue leads to severe neonatal hyperbilirubinemia in *UAC* mice. Since exons 3 and 4 encode the "common" region of the *Ugt1* locus, the other *Ugt1a* genes are also inactivated. All mouse experiments and procedures are in accordance with the Guide for the Care and Use of Laboratory Animals and were approved by the Univesity of California, San Diego Animal Care Committee.

Molecular Pharmacology Fast Forward. Published on October 19, 2015 as DOI: 10.1124/mol.115.098228
This article has not been copyedited and formatted. The final version may differ from this version.

Immunoblotting: Liver (MLM) and small intestinal microsomes (MSIM) from mice were prepared as previously described (Chen et al., 2013). All Western blots were performed by using NuPAGE 4-12% BisTris-polyacrylamide gels as outlined by the supplier (Invitrogen). Following transfer of the proteins, membranes were blocked with 5% nonfat dry milk in Tris-buffered saline for 1 hour and then incubated with primary antibodies in Tris-buffered saline overnight. Membranes were washed and incubated with horseradish peroxidase-conjugated secondary antibody for 1 hour. Antibodies used were a rabbit anti-human UGT1A1 (Chen et al., 2013) and a mouse anti-bovine myelin basic protein (BioRad #MCA409S). Both antibodies cross reacted with the mouse proteins. The conjugated horseradish peroxidase was detected using the ECL plus Western blotting detection system (Amersham Biosciences) and visualized by the BioRad gel documentation system.

Bilirubin glucuronidation assays: Bilirubin glucuronidation activity assay was performed as described previously (Chen et al., 2013). In brief, MLM or MSIM were incubated with different concentrations of bilirubin in reaction buffer containing 2 mM UDP-glucuronic acid (UDPGA). All reactions were performed in the dark. Bilirubin di-glucuronide formation was determined by liquid chromatography Alliance 2695 (Waters, MA) coupled to tandem mass spectrometry (API 4000 Applied Biosystems, Canada). The HPLC system used was equipped with a 50 × 3.2 mm Columbus C18 column (Phenomenex, Torrance, CA). Data are expressed as peak areas (AUC).

Total RNA Preparation and RNA Analysis by RT-PCR: Mouse tissues were collected and snap-frozen into liquid nitrogen, and then pulverized. Aliquots of the pulverized samples were homogenized in TRIzol (Invitrogen) for RNA isolation (Chen

Molecular Pharmacology Fast Forward. Published on October 19, 2015 as DOI: 10.1124/mol.115.098228
This article has not been copyedited and formatted. The final version may differ from this version.

et al., 2013). Reverse transcription (RT) was conducted by using iScript Reverse Transcriptase (BioRad) as outlined by the manufacturer. Following synthesis of cDNA, RT products were used for PCR reactions. Primer sequences for the *Ugt1a1* gene are presented in Chen et al. (2013). Real time PCR analysis of *Mrp* gene expression was conducted as previously described (Yueh et al., 2014) using forward (5-CCATCCAAGAAGACCCCACA-3') and reverse (5-CCCCTGTCACCGCTAAAGAA-3') primers.

Imunohistochemistry: Mice were anesthetized with Pentobarbital (40 mg/Kg, i.p.) and perfused through the right ventricle with 0.1 M phosphate buffer saline (PBS) (pH 7.4) followed by the same buffer containing 4% paraformaldehyde (PFA). Fixed tissues were post-fixed in 4% PFA in PBS for 72 h at room temperature (RT), dehydrated through a graded ethanol series and embedded in paraffin. For immunostaining, 3 µm sections were submitted to antigen retrieval in 20 mM citrate buffer with 1.5% H_2O_2 for 15 min at RT in the dark, incubated for 10 min in Tris/EDTA buffer at 84°C and blocked for 1 h at RT in 1% bovine serum albumin (BSA) in PBS. Primary antibodies, mouse-anti neurofilaments-medium (AbCam #ab7794, 1:50), rat-anti myelin basic protein (MBP) (AbDSerotec #MCA4095, 1:50) for oligodendrocyte and myelination detection, rabbit-anti glial fibrillary acidic protein (GFAP) (Sigma #G9269, 1:250) for astrocyte detection and rabbit-anti ionized calcium binding adaptor molecule (Iba)-1 (Wako #019-19741, 1:250) for microglial staining, were used in 0.5% BSA in PBS overnight at 4°C. For Purkinje cells staining, sections were blocked for 2 h at RT in 10% normal goat serum and 0.5% Triton X-100 in PBS and incubated overnight with mouse anti Adenomatus Polyposis Coli (CC-1) (Merck, # OP80) in 2% goat serum and 0.3% Triton X-100 in PBS. After washing in PBS, sections were incubated for 1 h at RT

Molecular Pharmacology Fast Forward. Published on October 19, 2015 as DOI: 10.1124/mol.115.098228
This article has not been copyedited and formatted. The final version may differ from this version.

with antibodies anti-mouse coupled to AlexaFluor 488 (Invitrogen #A11001, 1:1000) or anti-goat IgG (H+L) Cy3-conjugated (Jackson ImmunoResearch, #115-166-003, 1:3000), anti-rat coupled to AlexaFluor 568 (Invitrogen #A11077, 1:1000) or to AlexaFluor 488 (Invitrogen #A11006, 1:1000), and anti-rabbit coupled to Alexafluor 568 (Invitrogen #A11036, 1:1000) in 0.5% BSA in PBS, incubated for 20 min in DAPI and mounted with Shandon Immu-Mount™ Aqueous Non-fluorescing Mounting Medium (Thermo Scientific).

Tissue sections were visualized in an AxioImager Z1 fluorescence microscope equipped with 10x/0.30 Ph1, 20x/0.50 Ph2 and 40x/1.30 Oil Ph3 EC-Plan-Neofluar objectives (Carl Zeiss, Germany). Images were acquired with a MRm Axiocam ver 3.0 camera connected to a PC running the Axiovision 4 acquisition software (Carl Zeiss, Germany).

Measuring myelination and counting Iba1- and GFAP-labeled cells: In order to evaluate if kernicterus mice present alterations in brain morphology, axonal viability and myelination along several brain regions, sections were stained with neurofilament and MBP. To evaluate overall neuronal and myelination alterations, 10x magnification images were acquired and stitched using Microsoft image composite editor. Then binary masks were specified in ImgeJ software using the same cut-off intensity threshold value for each region of interest, defined as the minimum intensity due to specific staining above background values. Finally, the percentage of area immunoreactive for neurofilament and MBP was measured. In addition, it was also calculated the percentage of myelinated fibers obtained by the ratio of MBP to neurofilaments

Molecular Pharmacology Fast Forward. Published on October 19, 2015 as DOI: 10.1124/mol.115.098228
This article has not been copyedited and formatted. The final version may differ from this version.

staining. Moreover, changes in brain morphology were identified measuring the percentage of brain area occupied by cerebellum using the same software.

To evaluate more closely changes in myelination in the different brain areas, the percentage of area immunoreactive for neurofilament and MBP was measured in 40x magnification images, using binary masks as described before, in different brain regions (medulla oblongata, pons, cerebellum and corpus callosum) and in specific regions of cerebellum (white matter ramifications, middle of white matter tracts and white matter terminals).

To evaluate microglia and astrocytes, we determined the number of cells with positive staining for Iba-1 and GFAP, respectively, in the same regions that we evaluated myelination alterations. All results were given by averaging values determined in at least seven separate microscopic fields from three different sections from two control animals and three Kernicterus animals. Values are expressed as mean ± SEM.

Statistical analysis

All results are presented as mean ± SEM. Significant differences between two groups were determined by the two-tailed t-test performed on the basis of equal and unequal variance as appropriate and the P-values of * $p < 0.05$ and ** $p < 0.01$ were considered as statistically significant.

Molecular Pharmacology Fast Forward. Published on October 19, 2015 as DOI: 10.1124/mol.115.098228
This article has not been copyedited and formatted. The final version may differ from this version.

Results

Animal model development. Targeted deletion of the *Ugt1a1* gene and the *Ugt1* locus in mice was achieved by inserting a construct with the *PGK-neo* gene flanked by *Flp/FRT* recombinase sites and *Cre/loxP* recombinase sites flanking exons 3 and 4 of the *Ugt1a1* gene (Fig 1A). Breeding to homozygosity generates $Ugt1^{LoxP[FRTneoFRT]LoxP}$ or *UFP* mice. The *FRT* sites are positioned flanking the *PGK-neo* selection marker gene allowing for deletion of this DNA by Flp-recombinase, leaving the *LoxP* sites flanking exons 3 and 4 and generating $Ugt1^{LoxP/LoxP}$ or $Ugt1^{F/F}$ mice (Chen et al., 2013). Thus, the $Ugt1^{F/F}$ ($Ugt1^{LoxP/LoxP}$) mice are the same as *UFP* mice ($Ugt1^{LoxP[FRTneoFRT]LoxP}$) except the neomycin gene has been deleted. From previous studies, $Ugt1^{F/F}$ mice show normal levels of circulating TSB. However, characterization of *UFP* mice are hypomorphic for the *Ugt1a1* gene, with all of the neonatal mice displaying hyperbilirubinemia with TSB levels averaging around 2 mg/dl (Fig 1F). Hypomorphic gene expression is often seen following integration of targeting constructs through homologous recombination (Lewandoski, 2001). In *UFP* mice, hypomorphic expression of the *Ugt1a1* gene is not lethal, with neonatal and adult mice displaying elevated TSB levels. Hypomorphic *Ugt1a1* gene expression in liver tissue from *UFP* mice confirmed a reduction in mature RNA transcripts (Fig 1B), which corresponded to a reduced UGT1A1 protein expression (Fig 1C) and bilirubin UGT activity (Fig 1D). Reduced *Ugt1a1* gene expression occurs in all tissues in *UFP* mice, with an example being displayed in small intestine (Supplement 1). Thus, the impact of inserting the targeting construct into the *Ugt1* locus leads to delayed *Ugt1a1* expression in all tissues.

Targeted deletion of the *Ugt1a1* gene and the *Ugt1* locus in liver tissue was achieved by crossing *UFP* mice with *albumin-Cre* transgenic mice, resulting in

Molecular Pharmacology Fast Forward. Published on October 19, 2015 as DOI: 10.1124/mol.115.098228
This article has not been copyedited and formatted. The final version may differ from this version.

UFP/albumin-Cre mice, which are termed *UAC* mice (Fig 1A). Expression of Cre-recombinase from the *albumin-Cre* transgene leads to the deletion of exons 3 and 4 in the liver tissue only of the *Ugt1a1* gene. Liver tissue from *UAC* mice at 14 days after birth have no mature UGT1A1 RNA (Fig 1B) or microsomal UGT1A1 protein as determined by Western blot analysis (Fig 1C), and no measureable bilirubin UGT activity (Fig 1D). Newborn *UAC* mice show high levels of TSB (Fig 1F) that peak around 14 days after birth. The elevated TSB levels in *UAC* mice eventually leads to a 95% lethality rate (Fig 1E). The neonatal *UAC* mice show visible signs of CNS toxicity prior to death, as evident from the appearance of tremors and seizures.

Alterations in brain morphology of kernicterus mice. When brains were isolated from 14-day old *UAC* mice a diffuse yellow staining (kernicterus) throughout the brain was apparent (Fig. 1G). When compared to *UFP* mice, which do not accumulate bilirubin in brain tissue, *UAC* mice had a reduced cerebellar volume, as previously shown in humanized *UGT1* mice (Fujiwara et al., 2010) as well as in the Gunn rat model (Conlee and Shapiro, 1997). When saggital brain sections were immunostained (Figure 2), marked reduction of the cerebellum was observed in *UAC* mice when compared with the *UFP* littermates. Haematoxylin Eosin (H&E) and Cresyl Violet (Nissl) staining were used to quantitate cerebellum size in UFP and UAC mice (Supplement 2). Interestingly, the global brain area is not affected, possibly due to an increased dimension of the cortex and midbrain on top of the cerebellum.

Kernicterus mice present axonal loss and decreased myelination. Brain sections were immunostained for neurofilaments and myelin basic protein (MBP) to calculate the percentage of brain area occupied by these markers. As depicted in Figure 2A, a

Molecular Pharmacology Fast Forward. Published on October 19, 2015 as DOI: 10.1124/mol.115.098228
This article has not been copyedited and formatted. The final version may differ from this version.

decrease in diseased *UAC* brain area occupied by neurofilament staining (0.80-fold ± 0.08, $p<0.05$) was observed when compared with brain tissue from *UFP* mice. When changes related with myelination were determined there was a more pronounced decrease in MBP positive staining along all brain regions (0.62 ± 0.04, $p<0.01$) which correlated with the percentage of myelinated fibers (0.74 ± 0.04, $p<0.05$) in *UAC* brain tissue. These findings indicated that kernicterus mice present a reduced number of viable axons with myelination impairment, which we speculate to derive from a decreased ability of oligodendrocytes to produce myelin.

To examine if the early onset of bilirubin toxicity in the cerebellum had an impact on myelin sheath formation, we examined the expression pattern of MBP at 5-days after birth when TSB levels are already dramatically elevated (Fig 2B). Immunocytochemistry analysis showed a reduction in myelination in newborn UAC mice when compared to healthy UFP mice. Real time PCR analysis has confirmed that expression of the *Mbp* gene in the cerebellum in UAC mice is significantly induced, possibly in response to the inflammatory insult initiated by elevated bilirubin levels. Interestingly, accelerated gene expression is followed by a significant reduction in MBP accumulation as shown by Western blot analysis, which correlates with reduced myelin sheath formation.

Kernicterus mice present reduced myelination and increased glial reactivity in cerebellum, medulla oblongata and pons. As changes in myelination along different brain regions were observed, brain regions that presented myelination at postnatal day 7 were examined. Changes in myelination in medulla, pons, cerebellum and corpus callosum were evaluated, the last as a positive control of myelination since it is one of the first myelinated areas of the brain (Sturrock, 1980). As depicted in Figure

Molecular Pharmacology Fast Forward. Published on October 19, 2015 as DOI: 10.1124/mol.115.098228
This article has not been copyedited and formatted. The final version may differ from this version.

3A and 4A, there was a decrease in the percentage of myelinated fibers in medulla (0.81 ± 0.03, $p<0.01$), and a more marked effect in pons (0.58 ± 0.03, $p<0.01$) and cerebellum (0.61 ± 0.04, $p<0.01$), with no effect on corpus callosum (Supplement Fig 3). Brain sections prepared from *UFP* mice show myelinated fibers that are long and thin, while in diseased *UAC* mice the MBP staining appears as fragmented fibers and myelin agglomerates, suggesting a destruction of the myelin sheath surrounding the axons. Interestingly, the corpus callosum maintains the long myelinated fibers even in the kernicterus mice, corroborating the absence of myelin changes in that area. It is known that astrocytes (Zhang et al., 2006) and microglia (Olah et al., 2012) cooperate to create a favorable environment for myelination, while upon myelination injury they are rapidly activated (Petzold et al., 2002). To examine if gliosis takes place in kernicterus brain, microglia and astrocyte reactivity were identified by Iba-1 and GFAP staining, respectively. As shown in Figure 3, the kernicterus mice presented a marked increase in both microglia and astrocytes in cerebellum, medulla and pons with no effect in the corpus callosum (Supplement Fig 3). Regarding microglia (Fig. 3B and 4B), the major increase was observed in cerebellum (3.75-fold ± 0.04, $p<0.01$), followed by pons (2.22-fold ± 0.07, $p<0.01$) and medulla (1.68-fold ± 0.21, $p<0.05$). Concerning astrocytes, very similar increases were observed in medulla and cerebellum (3.73-fold ± 0.17, $p<0.05$ and 3.95-fold ± 0.08, $p<0.01$, respectively), but the most pronounced effects were noticed in pons (29.08-fold ± 3.93, $p<0.01$). Regarding the corpus callosum, this region with a considerable number of glial cells in the control animals showed no noticeable changes in the kernicterus mice.

Distinct white matter regions from cerebellum present different alterations in myelination and glial reactivity. Since cerebellum is one of the most affected areas

Molecular Pharmacology Fast Forward. Published on October 19, 2015 as DOI: 10.1124/mol.115.098228
This article has not been copyedited and formatted. The final version may differ from this version.

and it seems to present regional changes in myelination and glial reactivity, the cerebellum was divided into three distinct zones as depicted in Figure 5A; the white matter nodes (region 1), the middle of the white matter tracts (region 2), and white matter terminals (region 3). When myelination was evaluated (Fig. 5B and 6B) there was a marked decrease in the percentage of myelinated fibers in the kernicterus mice. The major effects were observed at white matter terminals (0.45-fold ± 0.07, $p<0.01$), followed by central white matter tracts (0.58-fold ± 0.04, $p<0.01$) and finally, a less pronounced but significant alteration was observed in white matter nodes (0.72-fold ± 0.05, $p<0.05$).

When the number of glial cells in these regions were evaluated there was a marked increase in both astrocyte and microglia number in cerebellum white matter of kernicterus mice (Fig. 5C, D and 6 C, D). In this context, there was an increased number of microglia in all three regions with a similar pattern to what was observed for myelination. Indeed, the most affected area was the white matter terminals (5.37-fold ± 0.18, $p<0.01$), followed by central white matter tracts (5.05-fold ± 0.27, $p<0.01$) and white matter nodes (3.11 ± 0.17, $p<0.01$). On the other hand, when astrocyte number was evaluated, kernicterus mice presented a very similar increase in both white matter nodes and terminals (3.36-fold ± 0.18, $p<0.01$ and 3.31-fold ± 0.25, respectively, $p<0.01$), with the most affected area being the central white matter (4.28-fold ± 0.15, $p<0.01$).

It deserves to be noted that while white matter terminals were the most affected area pertaining to changes in myelination and microgliosis, the changes in astrogliosis were mainly observed in the middle of the white matter tracts, possibly suggesting a different role for microglia and astrocytes in response to UCB injury.

Molecular Pharmacology Fast Forward. Published on October 19, 2015 as DOI: 10.1124/mol.115.098228
This article has not been copyedited and formatted. The final version may differ from this version.

Kernicterus mice present cerebellum atrophy and a great reduction in Purkinje cell number. Besides changes observed in myelination and glial reactivity, the cerebellum volume is greatly reduced in kernicterus animals, a feature also observed in Gunn rats that were traumatized by sulfadimethoxine administration to increase TSB levels (Conlee and Shapiro, 1997). As depicted in Figures 2 and 7A, *UAC* mice present a marked derangement of cerebellar lobules resulting in a greater reduction in the area occupied by cerebellum when compared with total brain area (0.45-fold ± 0.03, $p<0.01$). This cerebellum atrophy in kernicterus mice can be due to a massive reduction in the number of Purkinje cells (0.21-fold ± 0.03, $p<0.01$) mainly in the anterior lobes, and shrinkage of molecular and granular layers, as shown in Figure 7A. Purkinje cells that remained in the kernicterus brains (Fig. 7A) presented an altered morphology with reduced number of branches suggesting that cerebellar neuronal circuitry may be markedly affected.

Molecular Pharmacology Fast Forward. Published on October 19, 2015 as DOI: 10.1124/mol.115.098228
This article has not been copyedited and formatted. The final version may differ from this version.

Discussion

These findings confirm that deletion of the *Ugt1a1* gene and the *Ugt1* locus in liver tissue from *UAC* mice presents an animal model of severe hyperbilirubinemia that develops into BIND and kernicterus, leading to marked cerebellar hypoplasia in parallel with a reduction of myelination and an increase in astrogliosis and microgliosis in the cerebellum, pons and medulla oblongata. The inclusion of the targeting construct into the *Ugt1a1* gene led to a hypomorphic allele, resulting in altered *Ugt1a1* gene expression in all tissues and a condition of mild hyperbilirubinemia. Selectively targeting the deletion of the *Ugt1a1* gene in liver tissue exacerbates this condition, driving TSB levels to toxic concentrations that induce gliosis. Unlike *hUGT1* mice were the percentage of seizures and lethality is observed in 5-10 percent of the neonates, over 95% of the neonatal mice develop acute signs of brain damage when the liver *Ugt1a1* gene is targeted, as observed in *UAC* mice. It should be noted that $Ugt1^{F/F}$ mice do not develop neonatal hyperbilirubinemia (Chen et al., 2013), and deletion of the *Ugt1a1* gene in liver ($Ugt1^{\Delta Hep}$) produces minimal hyperbilirubinemia. The dramatic difference in TSB levels between $Ugt1^{\Delta Hep}$ and *UAC* mice is attributed to reduced UGT1A1 expression in extrahepatic tissues in the *UAC* mice.

It has been demonstrated that UCB impairs oligodendrocyte differentiation and consequent myelination in vitro using dorsal-root ganglia-oligodendrocyte co-cultures (Barateiro et al., 2013) and ex vivo in organotypic cerebellar slice cultures (Barateiro et al., 2012). These observations are consistent with previous reports showing a decrease in the density of myelinated fibers and a loss of axons in the cerebellum of a premature infant with kernicterus (Brito et al., 2012), along with white matter volume reduction and delayed hemispheric myelination as observed in infants with severe UCB encephalopathy (Gkoltsiou et al., 2008). In *UAC* mice, there was a marked impairment

Molecular Pharmacology Fast Forward. Published on October 19, 2015 as DOI: 10.1124/mol.115.098228
This article has not been copyedited and formatted. The final version may differ from this version.

of myelination. Indeed, fragmentation of myelinated fibers within the cerebellum, medulla oblongata and pons was detected, a finding which indicated that toxic levels of bilirubin led to damage of the myelin sheath. Myelination deficits have also been reported in several other perinatal conditions, including moderate perinatal systemic inflammation (Favrais et al., 2011), perinatal hypoxic-ischemia (Huang et al., 2009) and white matter injury in the premature baby (Buser et al., 2012). Since it is known that neuronal-oligodendrocyte cross-talk is crucial for proper myelination (Lee and Fields, 2009), myelination impairment observed in the kernicterus mice may be due in part to a reduced number of viable axons limiting oligodendrocyte differentiation and myelination. Nevertheless, the percentage of myelination in the remaining fibers was also affected in these animals corroborating the toxic role of bilirubin on oligodendrocyte maturation, as previously seen in several in vitro models. Actually, as reported for white matter injury (Buser et al., 2012), myelination failure may arise from the inability of oligodendrocyte precursors to generate myelinating oligodendrocytes in order to repair the injury.

It deserves to be noted that the increased astrogliosis and microgliosis in *UAC* mice overlay those brain areas that present myelin damage. This fact is more pronounced in the cerebellum (Fig. 4), where recruitment of both microglia and astrocytes in the surrounding white matter is induced. It is known that upon myelination damage both astrocytes and microglia are rapidly activated and migrate to the site of injury (Petzold et al., 2002) with sustained astrocyte presence along myelination (Miron et al., 2010;Petzold et al., 2002), even during the perinatal period (Buser et al., 2012;Huang et al., 2009). Upon demyelination, microglia are responsible for clearing myelin debris to allow for proper re-myelination (Olah et al., 2012). In addition, astrocytes and microglia produce growth factors that can facilitate oligodendrocyte

Molecular Pharmacology Fast Forward. Published on October 19, 2015 as DOI: 10.1124/mol.115.098228
This article has not been copyedited and formatted. The final version may differ from this version.

survival, differentiation and the ability to myelinate (Zhang et al., 2006;Stankoff et al., 2002;Olah et al., 2012), creating a favorable environment for repair. Indeed, we observed an acute increase in the number of microglia in the most affected areas of myelin deficits suggesting that these cells have been recruited to clear the damaged myelin. In the cerebellum where myelin sheath formation is inhibited, *Mbp* gene expression was significantly induced, possibly in response to the inflammatory insult in this brain region and the production of reactive oxygen species, or even as a compensatory response to the lack of functional MBP which has been degraded as a result of intense gliosis.

It can also be argued that if activated, microglia and astrocytes may release high amounts of proinflammatory mediators that are known toxicants for oligodendrocytes and their progenitors. This was observed in *hUGT1* mice and *hUGT1/Trl2*$^{-/-}$ mice that seizure, and show distinct glial cell activation (Yueh et al., 2014). It has been shown that activated microglia induced Purkinje neuronal death through TNF-α and IL-1β signaling (Kaur et al., 2013). Thus, myelination impairment and loss of Purkinje cells in the *UAC* mice may be due to oligodendrocyte damage by glial-derived inflammatory factors. In addition, it has been reported that following white matter injury in the premature, astrogliosis extended into the site of injury causing inhibition of oligodendrocyte differentiation and consequent myelination as a result of hyaluronic acid production (Buser et al., 2012). Interestingly, our results show increased astrogliosis in cerebellum central white matter tracts, which are regions that do not present the highest levels of myelination defects but are the most affected nerve fibers at white matter terminals. Thus, in the kernicterus model astrogliosis may be impairing re-myelination following myelin damage.

Molecular Pharmacology Fast Forward. Published on October 19, 2015 as DOI: 10.1124/mol.115.098228
This article has not been copyedited and formatted. The final version may differ from this version.

Cerebellar hypoplasia was the more marked feature observed in the kernicterus mice, as also demonstrated with a similar *Ugt1*$^{-/-}$ mouse model (Bortolussi et al., 2015). In a single case of a preterm infant that was diagnosed with kernicterus, histological analysis revealed a loss of myelin fibers in the cerebellum (Brito et al., 2012), indicating similarity with kernicterus in humans and our mouse model. Indeed, these findings revealed that increased circulating levels TSB derange cerebellar lobules, with a reduction of the thickness of the molecular and granular layers, and a marked loss of Purkinje cells that coincides with reduced branching of the remaining cells. Similar features were noted in Gunn rats (O'Callaghan and Miller, 1985;Conlee and Shapiro, 1997). The rodent cerebellar lobules mature postnatally, increasing over 20-fold from birth to 21 postnatal days. Interestingly, the cells within the ventral lobes, namely Purkinje cells, mature first followed by those in the anterior lobes (Altman, 1969), and may be susceptible to toxic levels of bilirubin. In *UAC* mice there is an increased loss of Purkinje cells in the anterior lobe. This finding suggests that elevated bilirubin levels early in the neonatal stages drives toxicity towards those regions of the CNS that are underdeveloped. This fact may be corroborated by earlier findings showing that immature neurons and astrocytes are more susceptible to UCB toxicity and cell death than mature ones (Falcao et al., 2006).

The cerebellum is a region of the brain that plays an important role in motor control, and contributes towards coordination, precision, and timing of movements (Fine et al., 2002). Therefore, damage to the cerebellum, as observed in *UAC* mice, may justify the abnormal motor control, movements and muscle tone observed in these mice, as well as in *hUGT1* mice (Fujiwara et al., 2010;Vogel et al., 2011). Similar motor deficits were observed clinically in severe neonatal hyperbilirubinemia (Shapiro, 2010). Interestingly, in *UAC* mice we also show alterations in several brain regions that are

commonly affected in human neonatal brains that develop kernicterus (Bhutani and Stevenson, 2011). Indeed, we have observed myelin deficits and gliosis in medulla oblongata and pons of kernicterus mice. Both medulla oblongata and pons are structures located on the brainstem, with the medulla being on the lower half of the brainstem, and the pons above the medulla yet below the midbrain and ventral to the cerebellum. The medulla oblongata connects the higher levels of the brain to the spinal cord and has an important role in the control of nervous system autonomic functions, including the reflex center of swallowing (Jean, 1984). Interestingly, a history of past or present suckling and swallowing dysfunction is often described in children with kernicterus (Shapiro, 2010), which may occur as a result of altered function of the medulla nerve cells as observed in our animal model.

Overall, our study reveals a new animal model of kernicterus showing anatomical and histological changes that may justify the clinical symptoms often detected in infants subjected to severe neonatal hyperbilirubinemia. Further studies will need to be conducted to examine the similarities and differences that occur in kernicterus syndrome from published reports in humans with those observed in our mouse model. However, we have identified deficits in myelination and enhanced gliosis in the kernicterus mice that are similar to findings in human brain sections, indicating that mechanisms responsible for the neurological dysfunction described in moderate to severe hyperbilirubinemia may be viewed as potential targets for new therapeutic strategies.

Molecular Pharmacology Fast Forward. Published on October 19, 2015 as DOI: 10.1124/mol.115.098228
This article has not been copyedited and formatted. The final version may differ from this version.

Acknowledgements.

Shujuan Chen and Andreia Baraterio contributed equally to this work. The authors would like to thank Glenn Handoko for excellent technical assistance.

Molecular Pharmacology Fast Forward. Published on October 19, 2015 as DOI: 10.1124/mol.115.098228
This article has not been copyedited and formatted. The final version may differ from this version.

AUTHOR CONTRIBUTIONS

Designed experiments:

Chen, Fernandes, Barateiro, Yueh, Nguyen, Tukey, and Brites.

Contributed reagents, materials and analytic tools:

Relvas, Olivier, Brites and Tukey.

Provided animals:

Tukey

Performed experiments:

Chen, Fernandes, Barateiro, Domingues, Olivier and Nguyen.

Performed data analysis:

Chen, Fernandes, Barateiro, Domingues, Relvas, Olivier, Tukey and Brites.

Wrote or contributed to the writing of the manuscript:

Fernandes, Chen, Yueh, Barateiro, Tukey, and Brites.

References

Altman J (1969) Autoradiographic and Histological Studies of Postnatal Neurogenesis. 3. Dating the Time of Production and Onset of Differentiation of Cerebellar Microneurons in Rats. *J Comp Neurol* **136**:269-293.

Barateiro A, Miron V E, Santos S D, Relvas J B, Fernandes A, Ffrench-Constant C and Brites D (2013) Unconjugated Bilirubin Restricts Oligodendrocyte Differentiation and Axonal Myelination. *Mol Neurobiol* **47**:632-644.

Barateiro A, Vaz A R, Silva S L, Fernandes A and Brites D (2012) ER Stress, Mitochondrial Dysfunction and Calpain/JNK Activation Are Involved in Oligodendrocyte Precursor Cell Death by Unconjugated Bilirubin. *Neuromolecular Med* **14**:285-302.

Bhutani VK and Stevenson D K (2011) The Need for Technologies to Prevent Bilirubin-Induced Neurologic Dysfunction Syndrome. *Semin Perinatol* **35**:97-100.

Bortolussi G, Codarin E, Antoniali G, Vascotto C, Vodret S, Arena S, Cesaratto L, Scaloni A, Tell G and Muro A F (2015) Impairment of Enzymatic Antioxidant Defenses Is Associated With Bilirubin-Induced Neuronal Cell Death in the Cerebellum of Ugt1 KO Mice. *Cell Death Dis* **6**:e1739.

Bosma PJ, Seppen J, Goldhoorn B, Bakker C, Oude E R, Chowdhury J R, Chowdhury N R and Jansen P L (1994) Bilirubin UDP-Glucuronosyltransferase 1 Is the Only Relevant Bilirubin Glucuronidating Isoform in Man. *J Biol Chem* **269**:17960-17964.

Brites D (2012) The Evolving Landscape of Neurotoxicity by Unconjugated Bilirubin: Role of Glial Cells and Inflammation. *Front Pharmacol* **3**:88.

Brito MA, Zurolo E, Pereira P, Barroso C, Aronica E and Brites D (2012) Cerebellar Axon/Myelin Loss, Angiogenic Sprouting, and Neuronal Increase of

Vascular Endothelial Growth Factor in a Preterm Infant With Kernicterus. *J Child Neurol* **27**:615-624.

Buser JR, Maire J, Riddle A, Gong X, Nguyen T, Nelson K, Luo N L, Ren J, Struve J, Sherman L S, Miller S P, Chau V, Hendson G, Ballabh P, Grafe M R and Back S A (2012) Arrested Preoligodendrocyte Maturation Contributes to Myelination Failure in Premature Infants. *Ann Neurol* **71**:93-109.

Chen S, Yueh M F, Bigo C, Barbier O, Wang K, Karin M, Nguyen N and Tukey R H (2013) Intestinal Glucuronidation Protects Against Chemotherapy-Induced Toxicity by Irinotecan (CPT-11). *Proc Natl Acad Sci U S A* **110**:19143-19148.

Cohen RS, Wong R J and Stevenson D K (2010) Understanding Neonatal Jaundice: a Perspective on Causation. *Pediatr Neonatol* **51**:143-148.

Conlee JW and Shapiro S M (1997) Development of Cerebellar Hypoplasia in Jaundiced Gunn Rats: a Quantitative Light Microscopic Analysis. *Acta Neuropathol* **93**:450-460.

Falcao AS, Fernandes A, Brito M A, Silva R F and Brites D (2006) Bilirubin-Induced Immunostimulant Effects and Toxicity Vary With Neural Cell Type and Maturation State. *Acta Neuropathol* **112**:95-105.

Favrais G, van de Looij Y, Fleiss B, Ramanantsoa N, Bonnin P, Stoltenburg-Didinger G, Lacaud A, Saliba E, Dammann O, Gallego J, Sizonenko S, Hagberg H, Lelievre V and Gressens P (2011) Systemic Inflammation Disrupts the Developmental Program of White Matter. *Ann Neurol* **70**:550-565.

Fine EJ, Ionita C C and Lohr L (2002) The History of the Development of the Cerebellar Examination. *Semin Neurol* **22**:375-384.

Fujiwara R, Nguyen N, Chen S and Tukey R H (2010) Developmental Hyperbilirubinemia and CNS Toxicity in Mice Humanized With the UDP Glucuronosyltransferase 1 (*UGT1*) Locus. *Proc Natl Acad Sci U S A* **107**:5024-5029.

Gkoltsiou K, Tzoufi M, Counsell S, Rutherford M and Cowan F (2008) Serial Brain MRI and Ultrasound Findings: Relation to Gestational Age, Bilirubin Level, Neonatal Neurologic Status and Neurodevelopmental Outcome in Infants at Risk of Kernicterus. *Early Hum Dev* **84**:829-838.

Huang Z, Liu J, Cheung P Y and Chen C (2009) Long-Term Cognitive Impairment and Myelination Deficiency in a Rat Model of Perinatal Hypoxic-Ischemic Brain Injury. *Brain Res* **1301**:100-109.

Jean A (1984) Brainstem Organization of the Swallowing Network. *Brain Behav Evol* **25**:109-116.

Johnson L and Bhutani V K (2011) The Clinical Syndrome of Bilirubin-Induced Neurologic Dysfunction. *Semin Perinatol* **35**:101-113.

Kaur C, Rathnasamy G and Ling E A (2013) Roles of Activated Microglia in Hypoxia Induced Neuroinflammation in the Developing Brain and the Retina. *J Neuroimmune Pharmacol* **8**:66-78.

Lee PR and Fields R D (2009) Regulation of Myelin Genes Implicated in Psychiatric Disorders by Functional Activity in Axons. *Front Neuroanat* **3**:4.

Lewandoski M (2001) Conditional Control of Gene Expression in the Mouse. *Nat Rev Genet* **2**:743-755.

Miron VE, Ludwin S K, Darlington P J, Jarjour A A, Soliven B, Kennedy T E and Antel J P (2010) Fingolimod (FTY720) Enhances Remyelination Following Demyelination of Organotypic Cerebellar Slices. *Am J Pathol* **176**:2682-2694.

Nguyen N, Bonzo J A, Chen S, Chouinard S, Kelner M, Hardiman G, Belanger A and Tukey R H (2008) Disruption of the *Ugt1* Locus in Mice Resembles Human Crigler-Najjar Type I Disease. *J Biol Chem* **283**:7901-7911.

O'Callaghan JP and Miller D B (1985) Cerebellar Hypoplasia in the Gunn Rat Is Associated With Quantitative Changes in Neurotypic and Gliotypic Proteins. *J Pharmacol Exp Ther* **234**:522-533.

Olah M, Amor S, Brouwer N, Vinet J, Eggen B, Biber K and Boddeke H W (2012) Identification of a Microglia Phenotype Supportive of Remyelination. *Glia* **60**:306-321.

Petzold A, Eikelenboom M J, Gveric D, Keir G, Chapman M, Lazeron R H, Cuzner M L, Polman C H, Uitdehaag B M, Thompson E J and Giovannoni G (2002) Markers for Different Glial Cell Responses in Multiple Sclerosis: Clinical and Pathological Correlations. *Brain* **125**:1462-1473.

Shapiro SM (2003) Bilirubin Toxicity in the Developing Nervous System. *Pediatr Neurol* **29**:410-421.

Shapiro SM (2005) Definition of the Clinical Spectrum of Kernicterus and Bilirubin-Induced Neurologic Dysfunction (BIND). *J Perinatol 2005 Jan ;25 (1):54 -9* **25**:54-59.

Shapiro SM (2010) Chronic Bilirubin Encephalopathy: Diagnosis and Outcome. *Semin Fetal Neonatal Med* **15**:157-163.

Stankoff B, Aigrot M S, Noel F, Wattilliaux A, Zalc B and Lubetzki C (2002) Ciliary Neurotrophic Factor (CNTF) Enhances Myelin Formation: a Novel Role for CNTF and CNTF-Related Molecules. *J Neurosci* **22**:9221-9227.

Stevenson DK, Dennery P A and Hintz S R (2001) Understanding Newborn Jaundice. *J Perinatol* **21 Suppl 1**:S21-S24.

Sturrock RR (1980) Myelination of the Mouse Corpus Callosum. *Neuropathol Appl Neurobiol* **6**:415-420.

Vogel A, Ockenga J, Tukey R H, Manns M P and Strassburg C P (2011) Genotyping of the UDP-Glucuronosyltransferase (UGT) 1A7 Gene Revisited. *Gastroenterology* **140**:1692-1693.

Yueh MF, Chen S, Nguyen N and Tukey R H (2014) Developmental Onset of Bilirubin-Induced Neurotoxicity Involves Toll-Like Receptor 2-Dependent Signaling in Humanized UDP-Glucuronosyltransferase1 Mice. *J Biol Chem* **289**:4699-4709.

Zhang Y, Taveggia C, Melendez-Vasquez C, Einheber S, Raine C S, Salzer J L, Brosnan C F and John G R (2006) Interleukin-11 Potentiates Oligodendrocyte Survival and Maturation, and Myelin Formation. *J Neurosci* **26**:12174-12185.

Molecular Pharmacology Fast Forward. Published on October 19, 2015 as DOI: 10.1124/mol.115.098228
This article has not been copyedited and formatted. The final version may differ from this version.

Footnotes

This work was supported by the National Institutes of Health National Institute of Environmental Health Sciences [ES010337], National Institute of General Medicine [GM100481, GM086713] and the National Cancer Institute [R21CA171008]. This work was also supported in part by the projects [PTDC/SAU-NEU/64385/2006] and iMed.ULisboa [UID/DTP/04138/2013], from Fundação para a Ciência e a Tecnologia (FCT). A. B. was a recipient of a PhD fellowship [SFRH/BD/43885/2008] from FCT. The funding organizations had no role in study design, data collection and analysis, decision to publish, or preparation of the manuscript.

Molecular Pharmacology Fast Forward. Published on October 19, 2015 as DOI: 10.1124/mol.115.098228
This article has not been copyedited and formatted. The final version may differ from this version.

Figure Legends

Figure 1. ***Generation and characterization of UFP and UAC mice***. A) The targeting construct *Ugt1a1*$^{loxP[FRTneoFRT]loxP}$ was electroporated into ES cells. The chimera mice were out-crossed with wild type C57BL/6 mice, and then in-bred to generate mice carrying the homozygous *Ugt1a1*$^{loxP[FRTneoFRT]loxP}$ allele (*UFP* mice). *UFP* mice were further bred into transgenic *Albumin-Cre* mice to generate *Ugt1a1*$^{F/F}$*/albumin-Cre* mice (*UAC* mice). B) RT-PCR of mouse *Ugt1a1* gene expression in liver tissue from mice with different genetic backgrounds. The primers crossed exon 1 to exon 5, generating a 1052 bp band for the intact *Ugt1a1* gene, and a 788 bp band for the *Ugt1a1* gene with exons 3 & 4 deleted as a result of Cre recombination. C) Mouse liver microsomes (MLM) were prepared from mice at 14 days old. Western blot analysis demonstrated that MLM from *UFP* mice had lower UGT1A1 protein expression levels, in comparison to wild-type (wt) MLM samples. No detectable UGT1A1 expression was observed in UAC livers. D) Bilirubin glucuronidation analysis was performed (mean ± SEM, **** $p<0.0001$, student t-test) by using MLM. E) The lethality associated with neonatal UAC mice during different developmental stages was studied. GraphPad Prism was used to prepare the survival curve and the statistical analysis. F) Blood samples were collected from both *UFP* and *UAC* mice at different developmental stages. Total serum bilirubin (TSB) was determined by using a bilirubinometer. Mice from at least three different cages were included at each time point. Student t-test was used to determine the statistical significance (* $p<0.05$, ** $p<0.01$). G) Brains were collected from UFP and UAC neonates at 15 days after birth. Yellow color as a result of bilirubin accumulation was observed in the brain from UAC mice.

Molecular Pharmacology Fast Forward. Published on October 19, 2015 as DOI: 10.1124/mol.115.098228
This article has not been copyedited and formatted. The final version may differ from this version.

Figure 2. ***Kernicterus mice present axonal loss and decreased myelination***. A) Serial sagittal images of Control and Kernicterus mice. Each image represents a montage of 100-150 images at 10x magnification. 3 μm brain sections of each animal were immunolabeled to identify neuronal axons (neurofilaments, green, middle panel) and myelin basic protein (MBP, red, bottom panel). Top panel represents the superposition of neurofilaments, MBP and DAPI staining, the last used for nuclei counterstain (blue). Scale bar represents 700 μm. B) Expression of MBP in cerebellum. RNA was used for real time PCR analysis and total cellular protein was used for Western blot analysis.

Figure 3. ***Reduced myelination and increased glial reactivity***. Representative images from cerebellum, medulla and corpus callosum from Control and Kernicterus mice immunolabeled to identify (A) neurons (neurofilament, red) and myelin basic protein (MBP, green), (B) microglia (Iba-1+ staining, red) and MBP (green) and (C) astrocytes (GFAP+ staining, red) and MBP (green). Nuclei were counterstained with DAPI dye (blue).

Figure 4. ***Reduced myelinated fibers and increased microglia and astroglia burden in the Kernicterus mice.*** Quantification of percentage of myelinated fibers (A) and the number of microglia (B) and astrocyte (C) per field in cerebellum, medulla, pons and corpus callosum from Control and Kernicterus mice. Results are mean ± SEM from two Control mice and three Kernicterus mice performed in triplicate. *$p<0.05$ *vs*. respective Control, **$p<0.01$ *vs*. respective Control.

Figure 5. ***Myelination and glial reactivity changes in Kernicterus mice***. (A) Three different regions were specified, Region 1 (white matter nodes), Region 2 (middle of

Molecular Pharmacology Fast Forward. Published on October 19, 2015 as DOI: 10.1124/mol.115.098228
This article has not been copyedited and formatted. The final version may differ from this version.

white matter tracts) and Region 3 (white matter terminals). Sections from Control and Kernicterus mice were immunolabeled to identify (B) neurons (neurofilament, red) and myelin basic protein (MBP, green), (C) microglia (Iba-1+ staining, red) and MBP (green) and (D) astrocytes (GFAP+ staining, red) and MBP (green). Nuclei were counterstained with DAPI dye (blue). Representative images from the three white mater regions are shown. Scale bar represents 25 µm.

Figure 6. ***Effect of Kernicterus on myelination, microglia and astrocyte density throughout white matter***. Graph bars represent the quantification of percentage of (A) total area occupied by neurofilaments, (B) myelinated fibers, (C) the number of microglia and (D) astrocytes per field in 3-different white matter regions (A, B and C) in the cerebellum from Control (*UFP*) and Kernicterus mice. Results are mean ± SEM from three Control mice and four Kernicterus mice performed in triplicate. *p<0.05 *vs.* respective Control, **p<0.01 *vs*. respective Control.

Figure 7. ***Kernicterus mice present cerebellum atrophy and loss of Purkinje cells***. (A) 3 µm sections of each animal were immunolabeled with Adenomatus Polyposis Coli (CC-1) to identify Purkinje cells and serial sagittal images were acquired from cerebellum of Control and Kernicterus mice. Each image represents a montage of 25-50 images at 10x magnification. Nuclei were counterstained with DAPI dye (blue). Scale bar represents 700 µm. (B) Representative images of Purkinje cells morphology in Control and Kernicterus mice. Scale bar represents 700 µm.

Figure 1

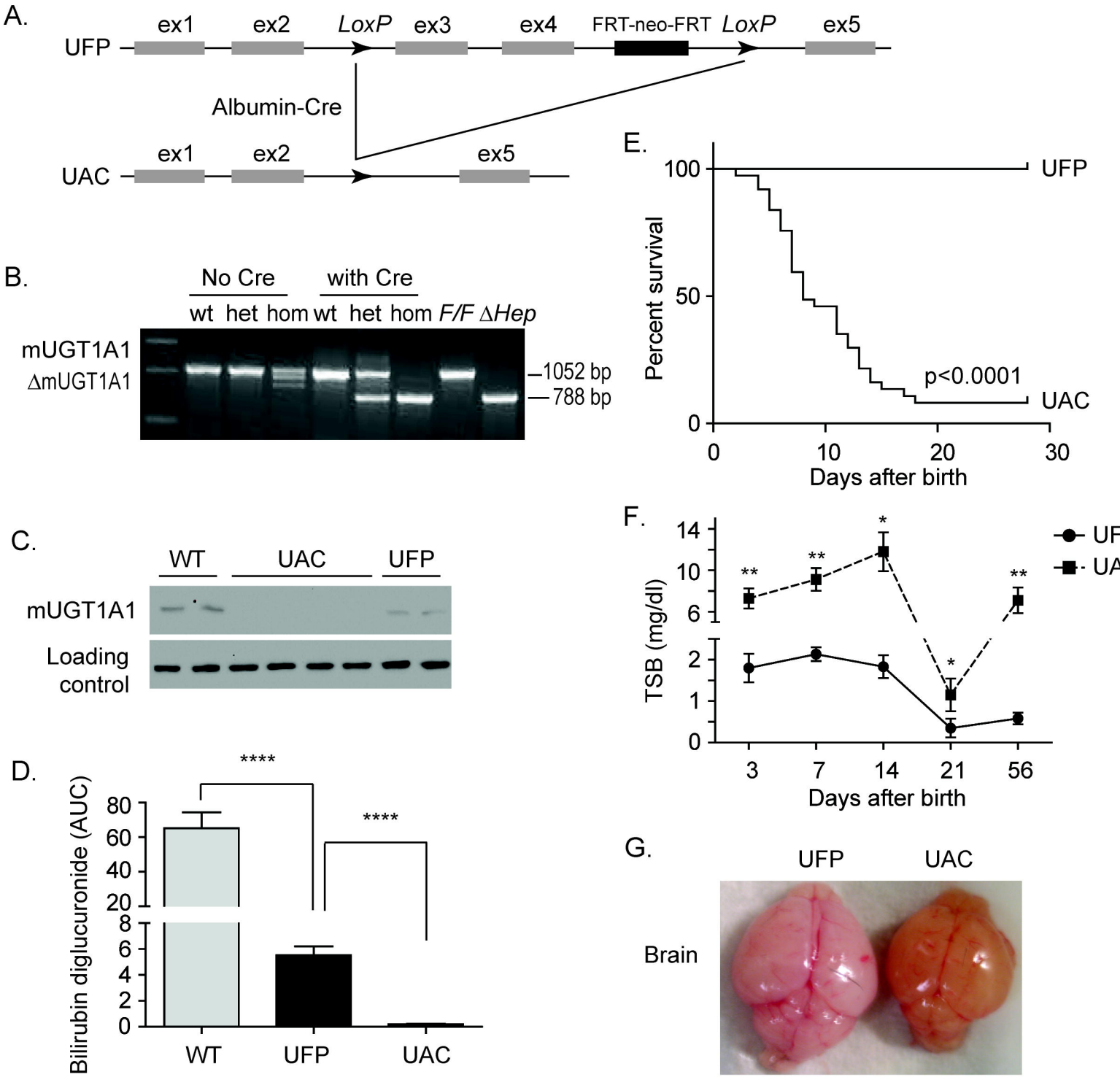

Molecular Pharmacology Fast Forward. Published on October 19, 2015 as DOI: 10.1124/mol.115.098228
This article has not been copyedited and formatted. The final version may differ from this version.

A

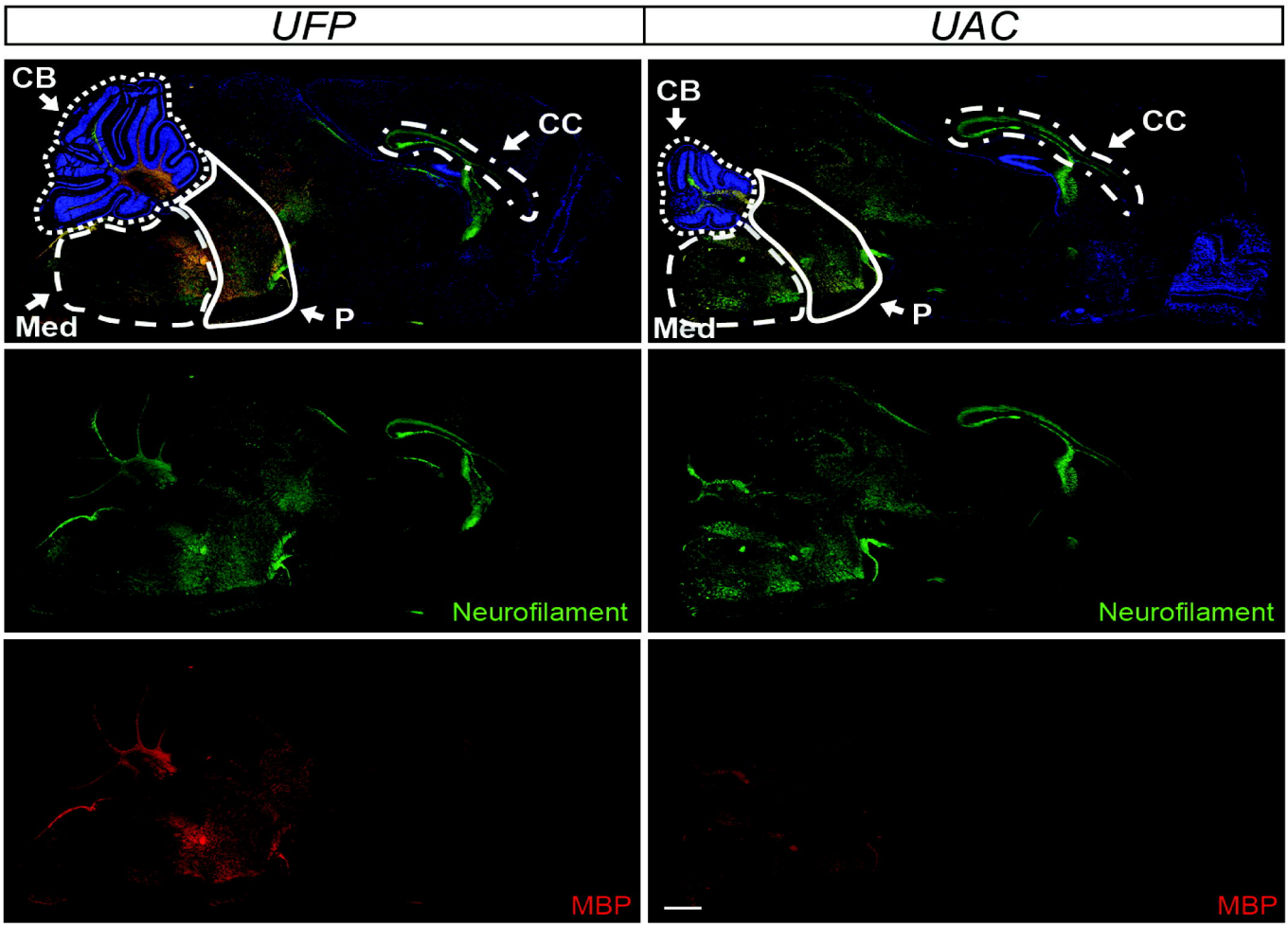

B

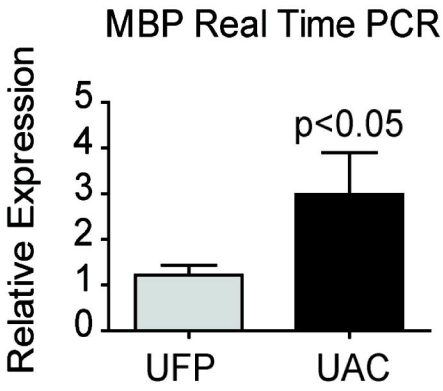

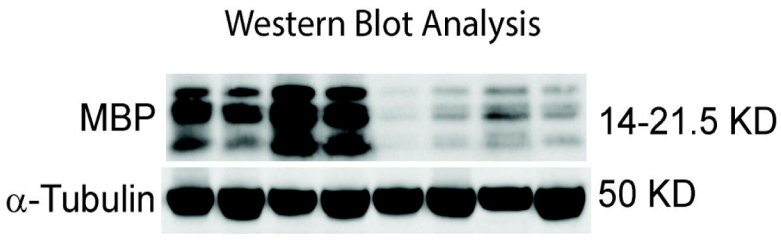

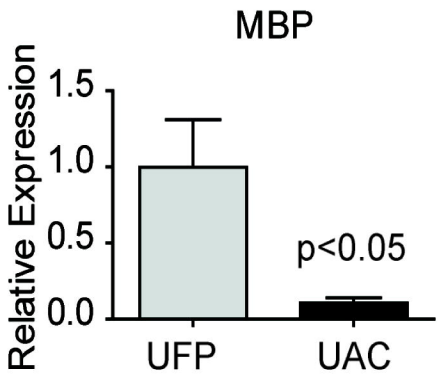

Figure 3

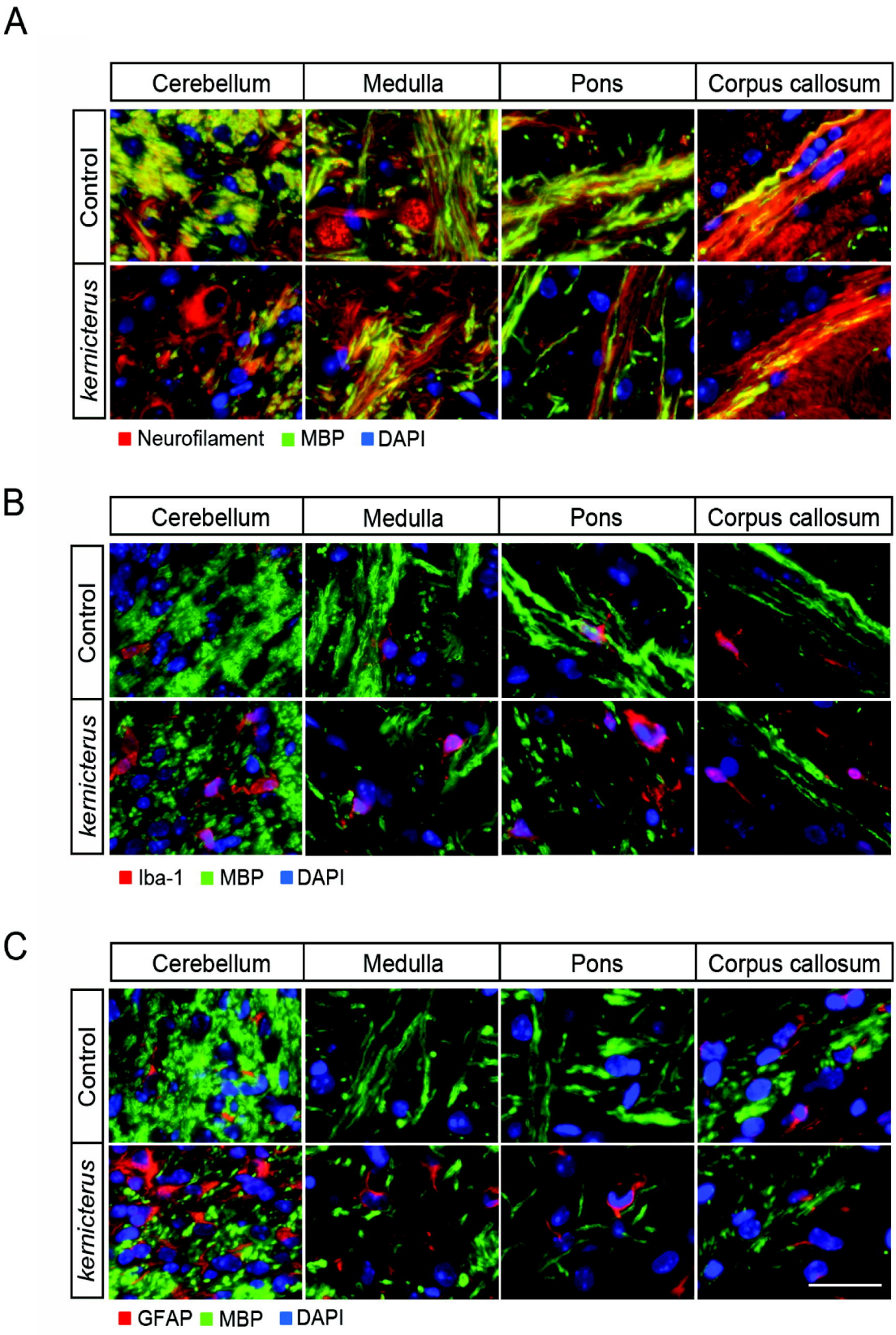
A
Cerebellum
Medulla
Pons
Corpus callosum
Control
kernicterus
Neurofilament
MBP
DAPI
B
Cerebellum
Medulla
Pons
Corpus callosum
Control
kernicterus
Iba-1
MBP
DAPI
C
Cerebellum
Medulla
Pons
Corpus callosum
Control
kernicterus
GFAP
MBP
DAPI

Figure 4

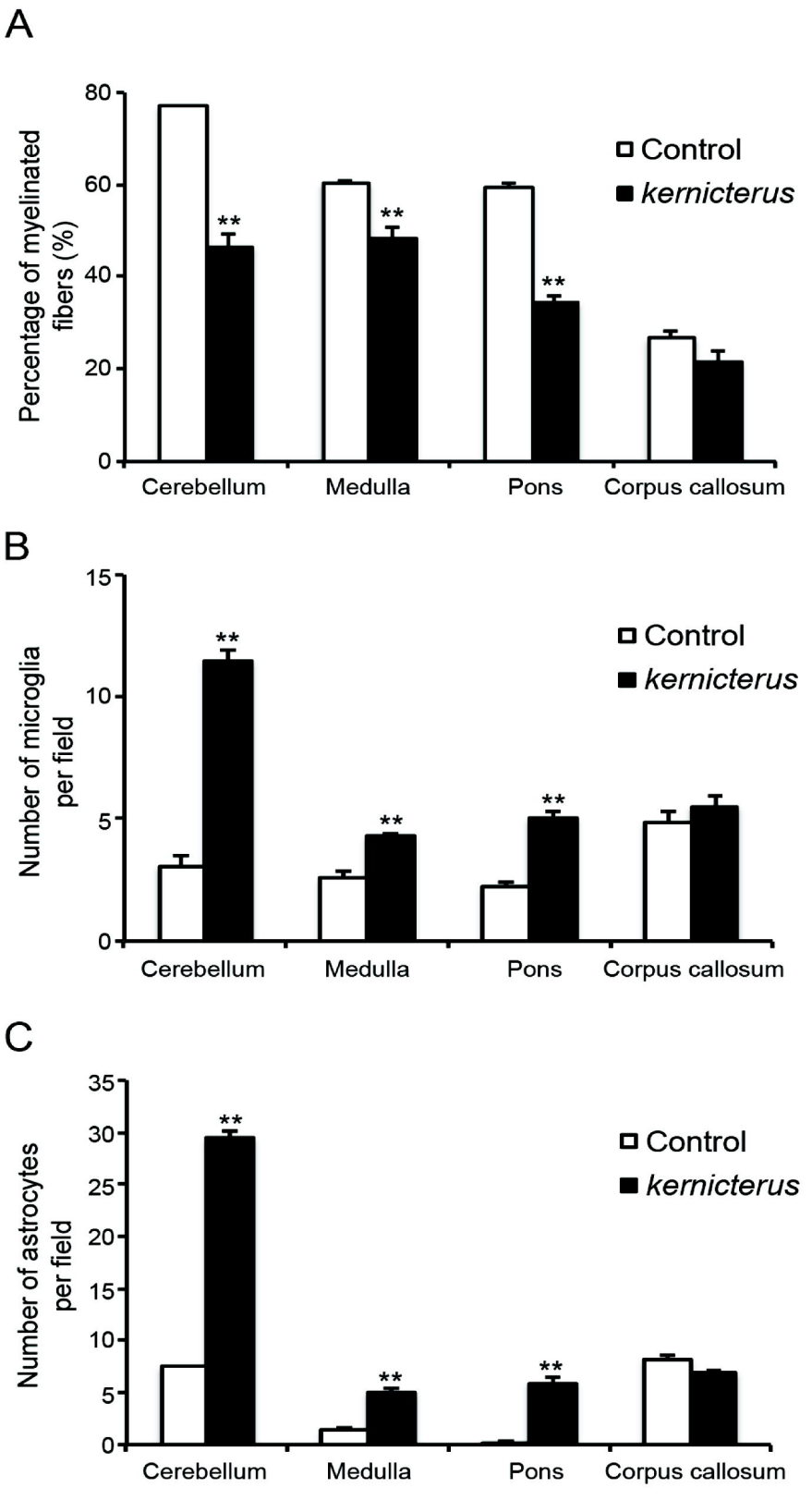
A
Percentage of myelinated fibers (%)
80
60
40
20
0
**
**
**
Control
kernicterus
Cerebellum
Medulla
Pons
Corpus callosum
B
Number of microglia per field
15
10
5
0
**
**
**
Control
kernicterus
Cerebellum
Medulla
Pons
Corpus callosum
C
Number of astrocytes per field
35
30
25
20
15
10
5
0
**
**
**
Control
kernicterus
Cerebellum
Medulla
Pons
Corpus callosum

Figure 5

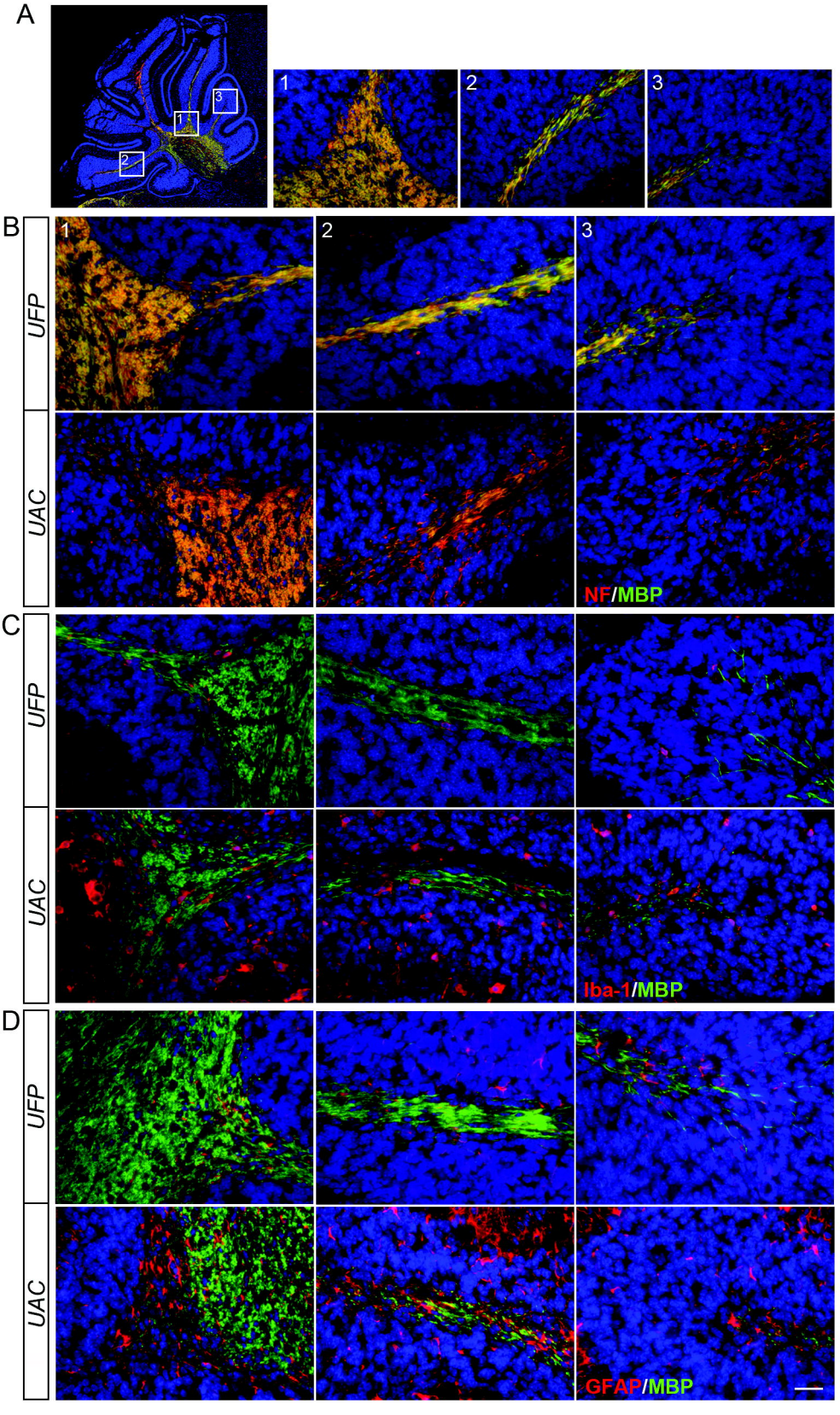

Figure 6

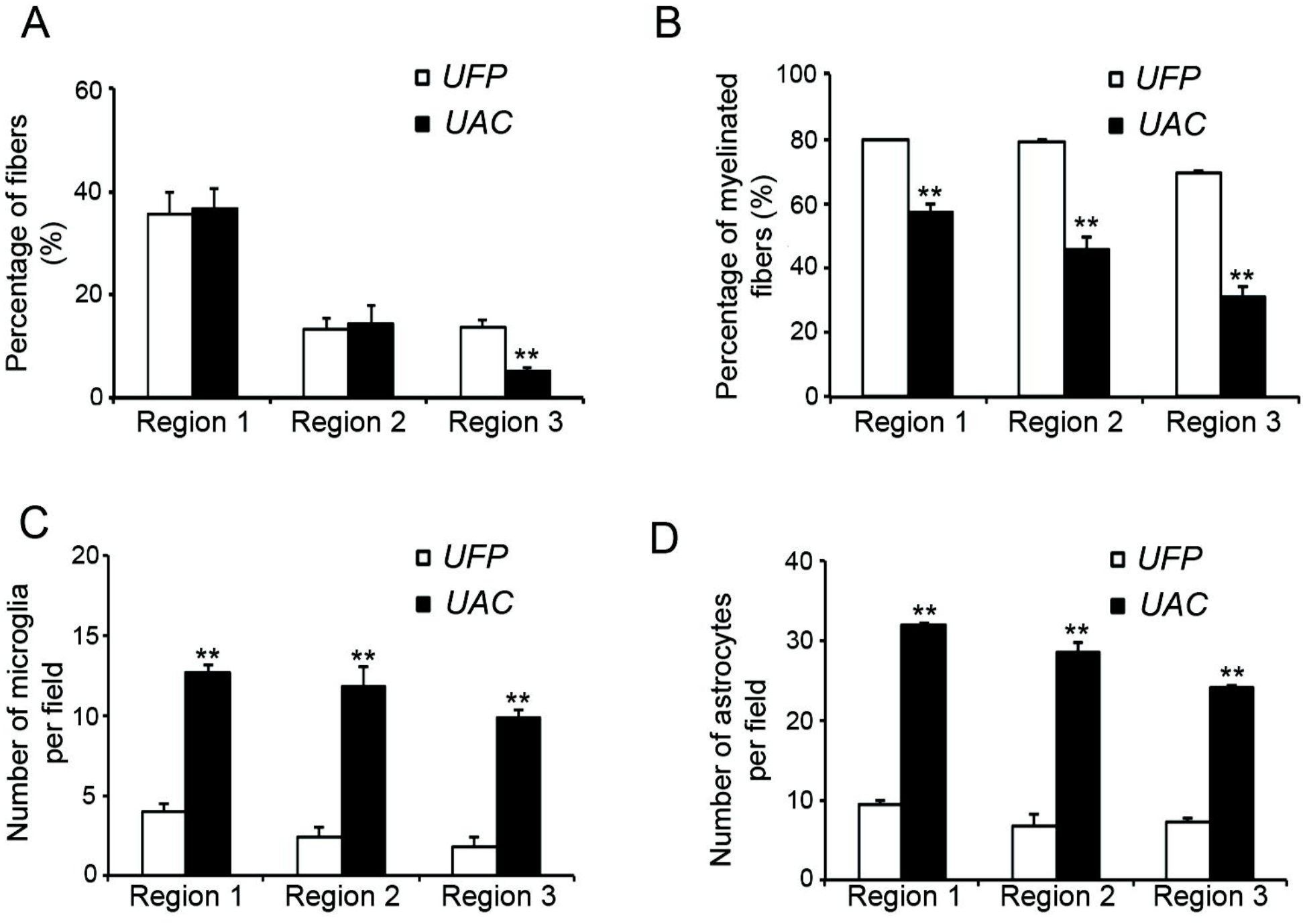
A
Percentage of fibers (%)
60
40
20
0
UFP
UAC
**
Region 1
Region 2
Region 3
B
Percentage of myelinated fibers (%)
100
80
60
40
20
0
UFP
UAC
**
**
**
Region 1
Region 2
Region 3
C
Number of microglia per field
20
15
10
5
0
UFP
UAC
**
**
**
Region 1
Region 2
Region 3
D
Number of astrocytes per field
40
30
20
10
0
UFP
UAC
**
**
**
Region 1
Region 2
Region 3

Figure 7